# Optical bistability based on Fano resonances in single- and double-layer nonlinear slab waveguide gratings

**Quang Minh Ngo,[1,3] Khai Q. Le,[2,4] Dinh Lam Vu,[1] and Van Hoi Pham[1]**

[1]*Institute of Materials Science, Vietnam Academy of Science and Technology, 18 Hoang Quoc Viet Road, Cau Giay, Hanoi, Vietnam*
[2]*Faculty of Science and Technology, Hoa Sen University, Ho Chi Minh City, Vietnam*
[3]*e-mail: minhnq@ims.vast.ac.vn*
[4]*e-mail: khai.lequang@hoasen.edu.vn*

Received January 23, 2014; revised March 6, 2014; accepted March 10, 2014; posted March 12, 2014 (Doc. ID 205292); published April 11, 2014

In this paper, we numerically investigate all-optical bistable switching at low input intensity based on Fano resonances available in nonlinear slab waveguide gratings with narrow slits. Fano resonances with various quality factors ($Q$-factors) in the single- and double-layer slab waveguide gratings are designed and their characteristics are studied by the finite-difference time-domain method. Dependencies on wavelengths of operation, various switching intensities, contrast, and bandwidth of all-optical bistabilities are observed. Comparing nonlinear characteristics of single- and double-layer grating configurations, the latter provides more bistable efficiency with the low input intensities needed and high contrast with high $Q$-factors at certain operating wavelengths. Both grating configurations in this work provide interesting venues for highly efficient Fano resonance-based all-optical bistable switching devices. 

*OCIS codes:* (050.6624) Subwavelength structures; (190.1450) Bistability; (130.3120) Integrated optics devices.
http://dx.doi.org/10.1364/JOSAB.31.001054

## 1. INTRODUCTION

The concept of optical bistable switching or bistability has been explored to implement all-optical transistors, switches, logical gates, and memory [1]. It has been employed widely in all-optical signal processing. In systems having optical bistability, the output intensity is a strong nonlinear function of the input intensity. These bistable systems might even display a hysteresis loop. One of the performance indicators of a bistable system is its ability to operate at low input intensity. Tremendous researches to realize all-optical bistable switching at low input intensity have been done. Among those, the utility of micro/nanophotonic structures in bistable systems, which enable strong light-matter interaction to enhance nonlinear effects of materials, has attracted much attention in integrated optics [2–9]. In addition, another important parameter needed to characterize a bistable switching is the $Q$-factor. All proposed structures for all-optical bistable switching at low input intensity particularly require high $Q$-factor. The micro/nanophotonic cavities with high $Q$-factors are of considerable interest and can be applied in extremely low-power nonlinear photonic devices because of their strong light-matter interactions. Natural materials normally have weak nonlinear effects, but when they are formed in particular structures, such as cavities having high $Q$-factors, they create qualitatively new phenomena. This will make nonlinearities of materials such as second harmonic generation and bistable switching become significantly stronger regardless of the low input intensity. Numerous micro/nanophotonic structures have been studied to realize all-optical bistable switching devices. Among those, bistable devices employing nonlinear photonic crystal cavities coupled to waveguides and slab waveguide gratings [2–9] are promising devices due to their potential on-chip applications. In our previous studies [6–8], we developed efficient all-optical bistable switching based on guided-mode resonances closed to Lorentzian line shapes in slab waveguide gratings and photonic crystal slabs, which are feasible designs due to their simple structures with easy in/out coupling and their cost-efficient process. However, since the $Q$-factor and shape of the Lorentzian guided-mode resonance strongly depend on the size, shape, and hole depths of slab waveguide gratings and photonic crystal slabs [6,7], its narrow linewidth corresponding to high $Q$-factor is difficult to design. Therefore, practical optical bistable switching devices working at extremely low input intensity may not be realized.

Fano resonance, as known from atomic physics, has been explored widely in various micro/nanophotonic structures, such as quantum dots [10], photonic crystals [11,12], plasmonic nanostructures, and metamaterials [13]. The interference of bright and dark modes in scattering spectra resulting in the so-called Fano resonance has been employed for a wide range of optical device applications [10]. Various applications of Fano resonance that rely on its high $Q$-factor due to its sharp and asymmetric profiles have been proposed, such as filters [14–16], modulators [5], sensors [17], broadband reflectors [18], and lasers [19]. Recently, Fano resonance has been explored in simple slab waveguide gratings with very narrow slits [20]. All-optical bistable switching characteristics based on Fano resonance may provide more bistable switching

 

efficiency than that based on guided-mode resonance (Lorentzian) in nonlinear slab waveguide gratings. With a given $Q$-factor, asymmetric profiles can provide sharper features than Lorentzian and, hence, allow more efficient input intensity. For filter applications, a double-layer stacked photonic crystal configuration can provide a $Q$-factor of Fano resonance over $10^7$ [15,16]. Fano resonance-based filters could achieve higher efficiency than other resonance-based ones. It has also been shown that Fano resonance-based filters with versatile spectral attributes can be implemented using double-layer slab waveguide gratings (DLSWG).

In [20], the switching intensity strongly depends on $Q$-factor and slit width. In order to reduce the switching intensity, $Q$-factor should be increased or slit width should be decreased to as narrow as possible. Due to the limitation of fabrication equipment and the cost, it is not an effective way to make optical bistable switching devices based on slab waveguide gratings with very narrow slits [21]. Therefore, it is crucial to explore efficient ways to reduce the switching intensity in the slab waveguide gratings. For this purpose, while keeping the slit widths, we propose here a DLSWG instead of a single-layer slab waveguide grating (SLSWG) for all-optical bistable switching applications. It appears that the resonant characteristics ($Q$-factor and resonant wavelength) of DLSWGs can be tuned when two slab waveguide grating components interact with each other. This interaction may happen in two possible routes, including a direct coupling and an indirect coupling of two slab waveguide gratings through gap-space propagation. Relying on relative coupling strengths, various resonant characteristics are achieved [22]. In addition, the $Q$-factor of the resonance in a SLSWG can be enhanced by increasing the thickness of the slab waveguide grating. However, the SLSWG offers limited dispersion engineering for tuning the output spectrum. In contrast, the DLSWG offers a flexible way to control the $Q$-factor, optomechanical interaction, and resonant wavelengths by varying the gap distance and the alignment between two layers [16]. To our best knowledge, there are no works using Fano resonances in DLSWGs for all-optical bistable switching. In this work, the all-optical bistable switching based on Fano resonances in both SLSWGs and DLSWGs is investigated. The switching intensity of each configuration is compared. We also show dependence of the operating wavelength on switching intensities and bistability behaviors for both configurations. The finite-difference time-domain method with subpixel smoothing for increased accuracy [23,24] has been used to carry out the calculations.

## 2. BISTABILITY IN SINGLE-LAYER GRATING DEVICES

Fano resonances can be simply obtained by using a SLSWG with narrow slits, as depicted in Fig. 1(a). In this case, a SLSWG structure whose guiding layer is chalcogenide glass ($As_2S_3$, $n = 2.38$) with a thickness ($d$) of 220 nm on a thick glass substrate ($n = 1.5$). The grating slit aperture ($w$) is formed by a rectangular corrugation in an $As_2S_3$ waveguiding layer with depth and periodicity ($\Lambda$) of 220 and 860 nm, respectively. A normally incident wave with transverse electric (TE) polarization is used. Perfectly matched absorbing boundary conditions are applied for the top and bottom boundaries of the computational unit cell while periodic boundary conditions are set at the left and right boundaries [23]. Figure 1(b) shows the calculated linear reflection spectra for three gratings with various slit widths of $w = 15$ nm, $w = 30$ nm, and $w = 45$ nm. An ultranarrow slit (~12 nm) can be fabricated [21], but it is at the border of current electron-beam lithography. In our optimized Fano resonance-based SLSWG design, a $Q$-factor of 14861 can be achieved with the slit width $w$ of 15 nm and the resonant peak at 1563.1 nm. As the slit width, $w$, increases, the resonance shifts to shorter wavelengths and the $Q$-factor of Fano resonance decreases dramatically. For instance, with the slit width, $w$, of 45 nm, the resonant peak and $Q$-factor are 1516.0 nm and 630, respectively. It means that, as the slit width increases, the waveguide mode gets more leaky and, hence, the linewidth becomes broader, leading to a decrease of $Q$-factor. Table 1 summarizes the linear characteristics of Fano resonance in SLSWGs. The linear characteristics can be explained similar to the guided-mode resonances in slab waveguide gratings and photonic crystal slabs [6,7]. The inset of Fig. 1(b) shows the electric field distributions of the resonant modes known as single grating modes.

In order to see all-optical bistable switching behaviors in SLSWGs with narrow slits, we excite an incident continuous wave (CW) source with suitable operating wavelength on the surface of the structure. In general, the operating wavelength is chosen approximately at the center of the all-optical bistability region. The nonlinear reflection spectra with the onset

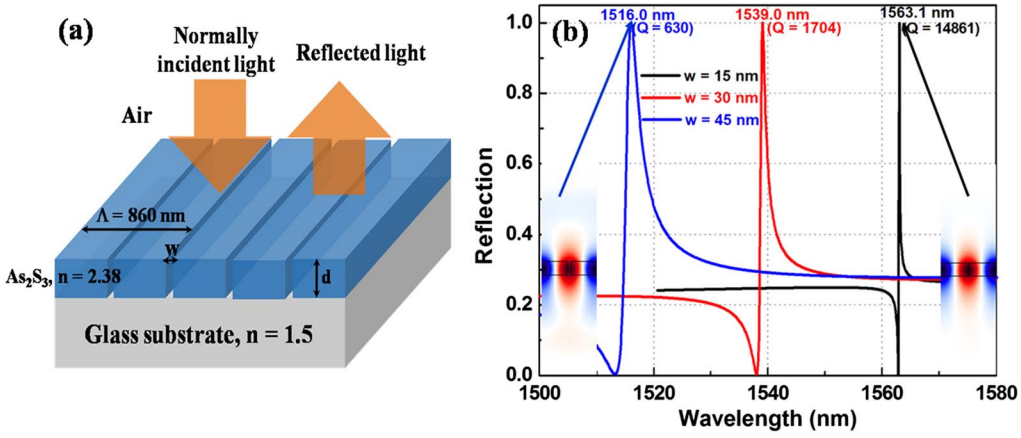


Fig. 1. (a) Sketch of a SLSWG with narrow slits under normally incident light. (b) Reflection spectra for various slit widths ($w$). The insets in (b) show the field distributions at resonances.

**Table 1. Linear Characteristics of SLSWGs and DLSWGs**

| | Single-Layer Gratings | | | Double-Layer Gratings | | |
|---|---|---|---|---|---|---|
| | $w = 15$ nm | $w = 30$ nm | $w = 45$ nm | $w = 15$ nm | $w = 30$ nm | $w = 45$ nm |
| Resonant peak (nm) | 1563.1 | 1539.0 | 1516.0 | 1331.0<br>1731.1 | 1314.3<br>1700.3 | 1301.1<br>1669.6 |
| $Q$-factor | 14861 | 1704 | 630 | 5066<br>18757 | 2518<br>2111 | 708<br>768 |

of optical bistability for several input intensities for Fano resonances are not shown here since they have already been described and discussed in [20]. In our calculations of all-optical bistable switching for SLSWGs with narrow slits, we choose the operating wavelengths at 50%, $1/e$, and 60% reflection, which locate in the bistability region. In nonlinear calculations, the third-order nonlinear coefficient of $As_2S_3$ is $n_2 = 3.12 \times 10^{-18}$ m$^2$/W [25]. Figure 2 shows a dependence of reflection on the incident flux intensity of the all-optical bistable switching in the SLSWG, with various narrow slits of (a) $w = 15$ nm, (b) $w = 30$ nm, and (c) $w = 45$ nm, respectively, for the operating wavelength at 50% reflection. It can be seen that the all-optical bistable switching behaviors are formed in all designs. The calculation technique to get the bistability behavior was discussed in [6–8]. The higher branch (blue curve, with $S_1$) is observed by increasing the incident flux intensity starting from low intensity. Following the higher branch, at the critical incident flux intensity the reflection decreases abruptly, which is referred to as the switching intensity. To observe the lower branch (red curve, with $S_2$), the incident flux intensity slowly decreases starting from the high intensity (above the switching intensity). When the incident flux intensity decreases over the switching intensity, the reflection remains in the lower branch due to the feedback of Kerr nonlinearity. It reaches slowly and surpasses the higher branch and jumps down abruptly to the high-reflection

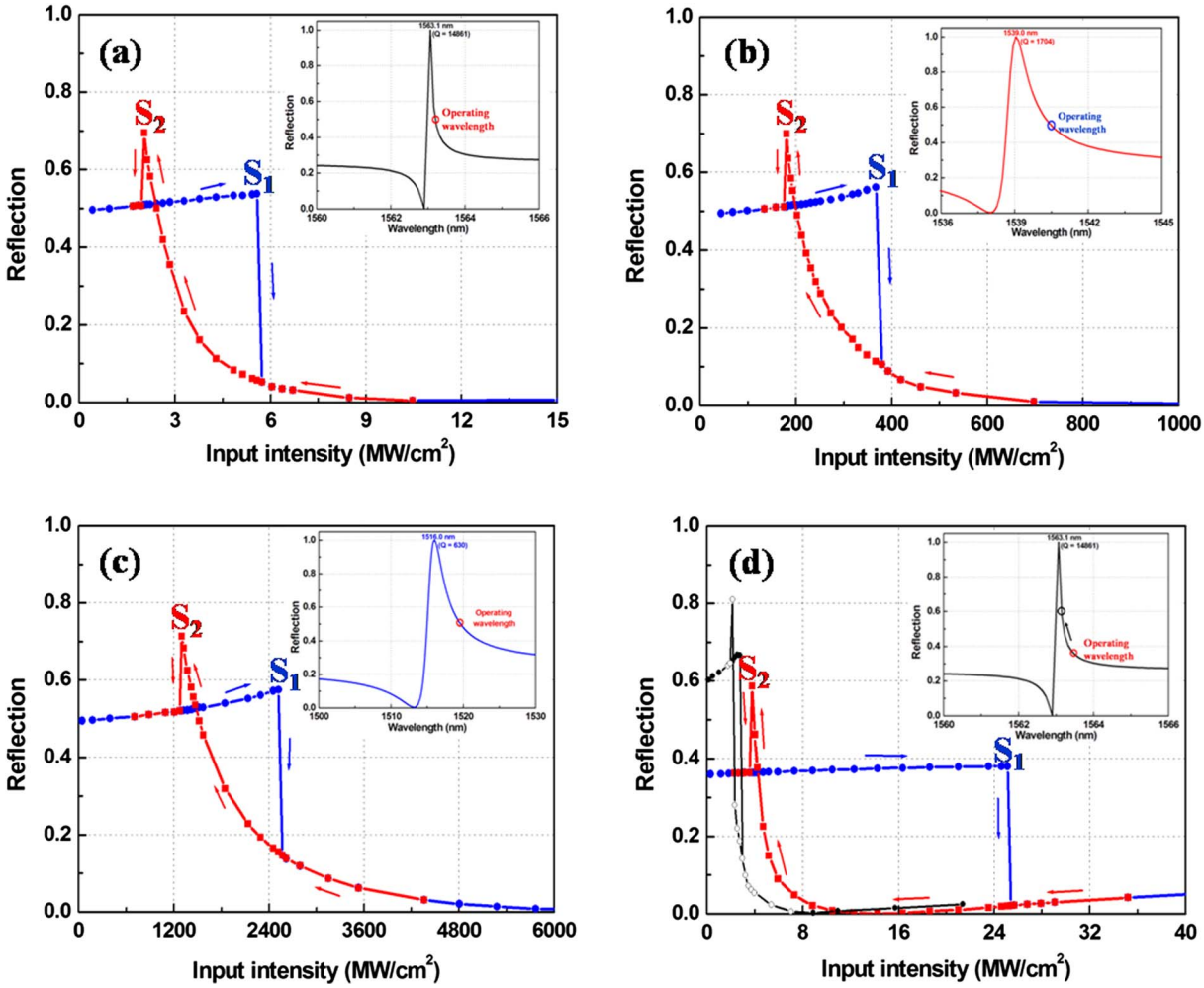


Fig. 2. All-optical bistable switching in the nonlinear SLSWGs depicted in Fig. 1(a) with the operating wavelength at 50% reflection (a) $w = 15$ nm, (b) $w = 30$ nm, (c) $w = 45$ nm, (d) operating wavelengths at $1/e$ [(blue, horizontal, with $S_1$) and (red, right vertical) curves] and 60% (black, left vertical curves) reflection for $w = 15$ nm.

state as the reflection reaches unity. In fact, the all-optical bistable switching behaviors have two switching points at the increasing ($S_1$) and decreasing ($S_2$) input intensities. That is the mechanism of bistability as in Fig. 2. The presence of $S_1$ and $S_2$ in these cases are due to the very short distance between the depths and peaks of the linear reflection spectra. The switching times are not mentioned in this work. The incident intensity for switching can be estimated as the input intensity for which the reflection decreases abruptly in the blue and red curves. For example, in Figs. 2(a)–2(c), the estimated switching intensities are 5.6 MW/cm$^2$, 366.1 MW/cm$^2$, and 2548.8 MW/cm$^2$ (at point $S_1$) and 2.0 MW/cm$^2$, 181.1 MW/cm$^2$, and 1306.4 MW/cm$^2$ (at point $S_2$), and the $Q$-factors are 14861, 1704, and 630 for the slit widths, $w = 15$ , 30, and 45 nm, respectively. These results also show the $1/Q^2$ dependence of the switching intensity. Figure 2(d) shows the all-optical bistable switching behaviors for the slit width, $w$, of 15 nm with the operating wavelengths at $1/e$ [blue (angular, with $S_1$) and red curves (with $S_2$)] and 60% (black curves, left) reflection. As seen in Fig. 2(d), the estimated switching intensities are about 25.2 MW/cm$^2$ and 2.6 MW/cm$^2$ (at point $S_1$) and 3.8 MW/cm$^2$ and 1.9 MW/cm$^2$ (at point $S_2$). The operating wavelength at 60% reflection seems to be a boundary and, at an operating wavelength lower than that, bistability behavior is observed. If the operating wavelength is more than 60% reflection, the bistability behavior disappears. Other SLSWGs ($w = 30$ and 45 nm), whose bistability behaviors for operating wavelengths at 60% and $1/e$ reflection are not shown here, exhibit the same tendency. Table 2 shows the optical switching intensity (at point $S_1$) and contrast (between the low and high reflection states of the bistability region) for SLSWGs with operating wavelengths at 50%, $1/e$, and 60% reflection. Compared to the result in Fig. 2(a), it can be seen that the more different the operating wavelength is from the resonance, the higher the switching intensity and the broader the bandwidth of the bistability region, because the detuning of the operating wavelength corresponds to the broad bandwidth and, thus, a higher amount of resonance shift is required to change the state. In addition, as long as the input intensity exceeds a certain value, the low-reflection state in the bistability region can be maintained. For example, for the slit width, $w$, of 15 nm, the bistability regions (between $S_1$ and $S_2$) are from 5.6 MW/cm$^2$ to 2.0 MW/cm$^2$, from 25.2 MW/cm$^2$ to 3.8 MW/cm$^2$, and from 2.6 MW/cm$^2$ to 1.9 MW/cm$^2$ for the operating wavelengths at 50%, $1/e$, and 60% reflection, respectively. Compared to the results presented in [20] with the operating wavelength at ~45% reflection for the slit width $w = 12$ nm, the performances of our SLSWG design for the slit width, $w = 15$ nm, are better in terms of higher $Q$-factor (2 times enhancement) and lower switching intensity at the $S_1$ point (~10 times and ~2 times reduction for the operating wavelengths at 50% and $1/e$ reflection, respectively). The temporal responses of the operating wavelength and the structure are not investigated here, but have shown the same tendency that we presented before in [6,7].

## 3. ALL-OPTICAL BISTABLE SWITCHING IN DOUBLE-LAYER GRATINGS

As mentioned above, all-optical bistable switching behaviors can be obtained based on Fano resonances in SLSWGs with very narrow slits. The switching intensity depends on the $Q$-factor and the shape of Fano resonances. The dependence of the switching intensity on the $Q$-factor is $1/Q^2$. To achieve a high $Q$-factor the slit width, $w$, must be decreased. Due to fabrication limitation, it is a big challenge to reduce the slit width, $w$, smaller than 12 nm. High $Q$-factor, however, can be achieved if two layers of slab waveguide gratings are stacked, as shown in Fig. 3(a). In these structures, the two slab waveguide gratings (thickness of each layer is 220 nm) with narrow slits considered in the previous section are separated by a thin silicon dioxide ($SiO_2$) buffer layer (20 nm). As the $SiO_2$ buffer layer is thin, two Fano resonances are coupled to form supermodes of even and odd symmetries. As a consequence, additional resonant peaks appear in the reflection spectrum. The $Q$-factor of the Fano resonance can be arbitrarily higher, relying on the relative phase retardation between two SLSWGs [15,22]. Figure 3(b) shows the linear reflection spectra for the slit widths, $w$, of 15 nm, 30 nm, and 45 nm, respectively. For each spectrum, there exists two Fano resonances, as shown in Figs. 3(c) and 3(d), respectively. The first Fano resonance (F1), at around 1300 nm, and the second one (F2), at around 1700 nm, correspond to the odd and even symmetry modes. The corresponding mode profiles are shown in insets of Figs. 3(c) and 3(d). The $Q$-factors of F1 for the slit widths, $w$, of 15 nm, 30 nm, and 45 nm are 5066, 2518, and 708, respectively. The $Q$-factors of F2 for the slit widths, $w$, of 15 nm, 30 nm, and 45 nm are 18757, 2111, and 768, respectively. The resonant peaks and $Q$-factors of the DLSWGs are also shown in Table 1. The blue (top) and red (bottom) colors indicate the characteristics of F1 and F2 for the double-layer gratings. In this work, the buffer layer's thickness influence on the $Q$-factor is not determined.

The all-optical bistable switching characteristics of the DLSWGs for F1 and F2 are also calculated. Figures 4(a) and 4(b) (blue/S1 and red/S2 curves) show the all-optical bistable switching behaviors of the DLSWGs as depicted in Fig. 3(a) for the slit widths of 15 nm and 45 nm for F1, with the operating wavelength at 50% reflection. The all-optical bistable switching behaviors of these cases are similar to the

**Table 2. Nonlinear Characteristics of SLSWGs**

| | Single-Layer Gratings | | |
|---|---|---|---|
| | $w = 15$ nm | $w = 30$ nm | $w = 45$ nm |
| Switching intensity–$S_1$ (MW/cm$^2$) and Contrast (low-high states) with operating wavelength at 50% reflection | 5.6 (0.05–0.54) | 366.1 (0.1–0.56) | 2548.8 (0.14–0.58) |
| Switching intensity–$S_1$ (MW/cm$^2$) and Contrast (low-high states) with operating wavelength at $1/e$ reflection | 25.2 (0.02–0.38) | 1526.0 (0.01–0.39) | 9950.6 (0.01–0.40) |
| Switching intensity–$S_1$ (MW/cm$^2$) and Contrast (low-high states) with operating wavelength at 60% reflection | 2.6 (0.11–0.65) | 171.1 (0.13–0.67) | 1235.3 (0.16–0.68) |

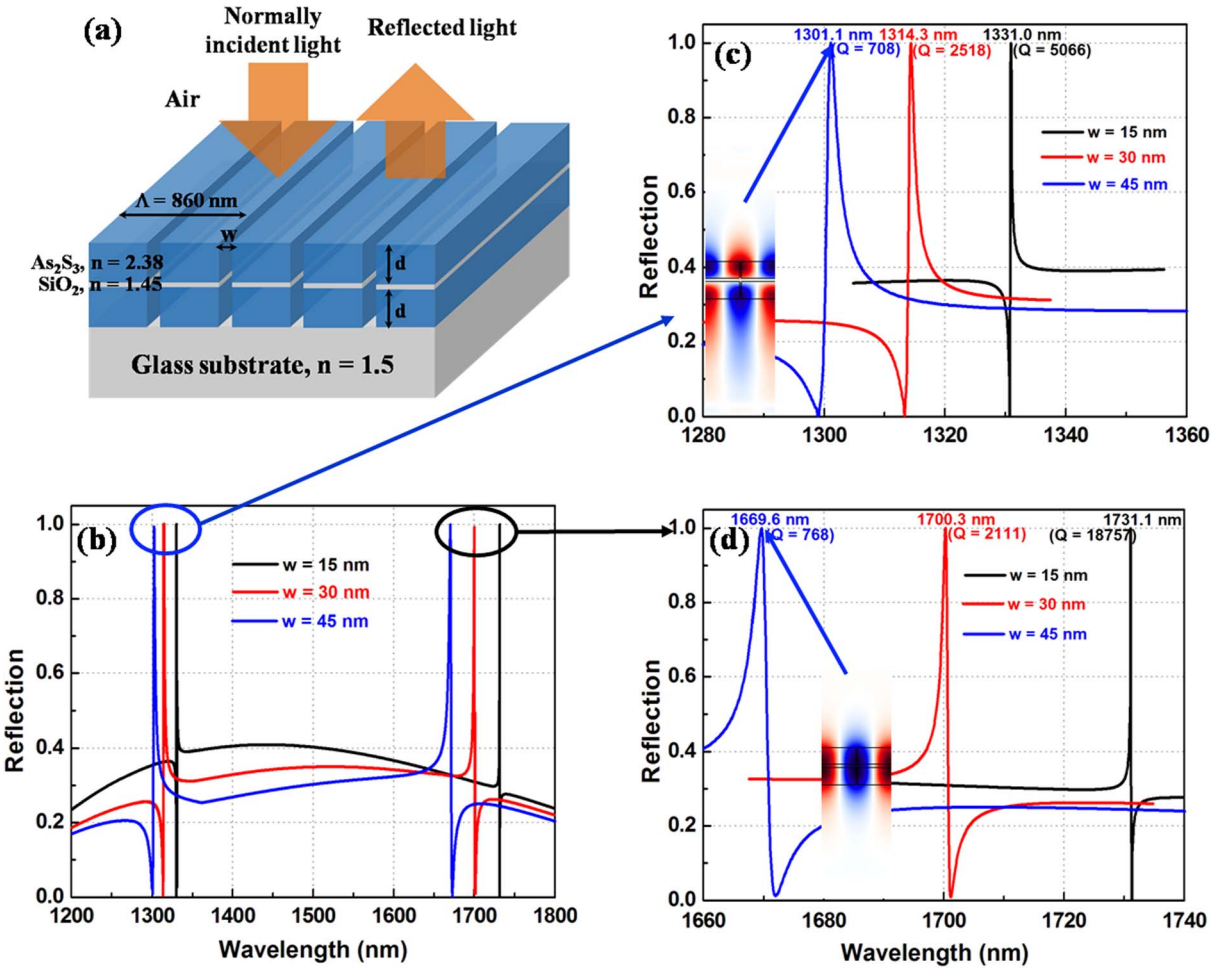


Fig. 3. (a) DLSWG with a 20 nm $SiO_2$ gap. (b) Reflection spectra for various slit widths ($w$). (c) and (d) enlarged resonant regions for the shorter and longer wavelength regions, respectively. The insets in (c) and (d) show the field distributions at resonances.

SLSWGs. For the operating wavelength at 50%, we can estimate the input intensities for switching to be 46.4 MW/cm$^2$ and 2299.8 MW/cm$^2$ at point $S_1$ and 19.6 MW/cm$^2$ and 253.7 MW/cm$^2$ at point $S_2$ for the slit widths, $w$, of 15 nm and 45 nm, respectively. We have also shown the bistability behaviors for the operating wavelength at 60% reflection as the black curves (that start at Reflections of 0.6) in Figs. 4(a) and 4(b), this operating wavelength seems to be a boundary. As seen in Figs. 4(a) and 4(b), the smaller switching intensity and bandwidth of the bistability region, the closer to the

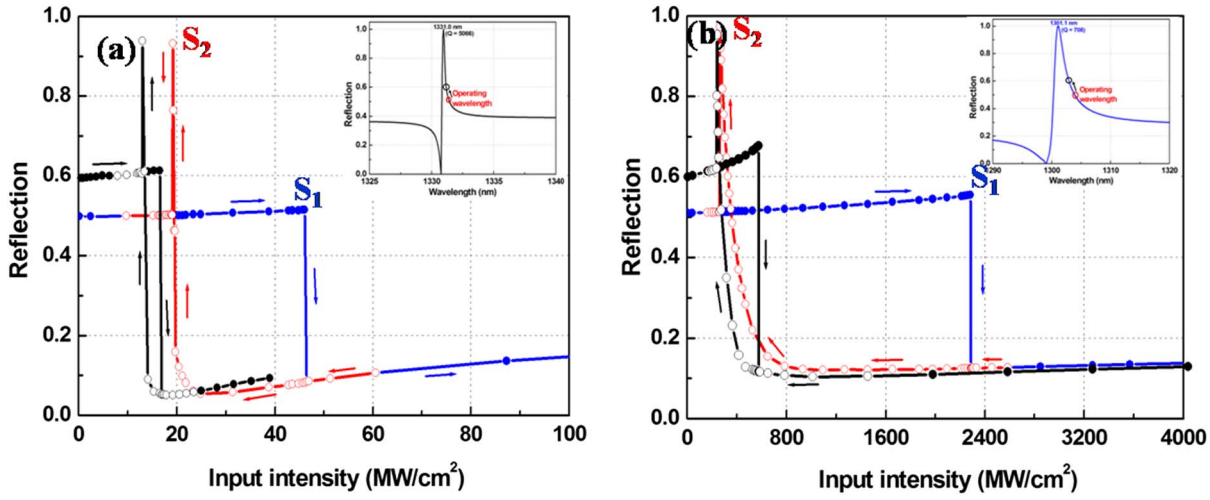


Fig. 4. All-optical bistable switching behaviors of the DLSWGs with (a) $w = 15$ nm and (b) $w = 45$ nm for the shorter resonant region with the operating wavelengths at 50% [blue (with $S_1$ and red (with $S_2$) curves] and 60% [black (left) curves] reflection.

**Table 3. Nonlinear Characteristics of DLSWGs for the Operating Wavelengths at the Shorter (F1) and Longer (F2) Resonant Wavelengths**

| | Double-Layer Gratings | | |
|---|---|---|---|
| | $w = 15$ nm | $w = 30$ nm | $w = 45$ nm |
| Switching intensity (MW/cm$^2$) and Contrast (low-high states) with shorter operating wavelength at 50% reflection | 46.4 (0.08–0.51) | 179.1 (0.1–0.53) | 2299.8 (0.12–0.56) |
| Switching intensity (MW/cm$^2$) and Contrast (low-high states) with shorter operating wavelength at 60% reflection | 16.5 (0.06–0.61) | 63.1 (0.08–0.64) | 561.1 (0.11–0.67) |
| Switching intensity (MW/cm$^2$) and Contrast (low-high states) with longer operating wavelength at 10% reflection | 1.92 (0.10–0.89) | 104.0 (0.07–0.97) | 733.5 (0.06–0.97) |

resonance of the operating wavelength it will be. The switching intensity and contrast of DLSWGs with the operating wavelengths at 50% and 60% reflection are shown in Table 3. Compared to the calculated result of SLSWGs, for the slit width of 15 nm and operating wavelength at 50% reflection, the $Q$-factor reduces by ~2.9 times and the switching intensity increases by ~8.3 times. For the slit width of 45 nm, the $Q$-factor slightly increases (708 compared to 630) and the switching intensity is lower than that from the single-layer grating. In general, bistable switching based on DLSWGs does not provide a more significant enhancement than those of SLSWGs for operating wavelengths at F1. However, for operating wavelengths at F2, it is seen from Table 3 that the DLSWGs provide better bistable switching performance in terms of higher $Q$-factors, lower switching intensity, and high contrast between high and low states than those from the SLSWGs for various slit widths.

Since the performance of bistable switching based on F2 is better than that based on F1, the following bistable switching investigations are carried out for various operating wavelengths around F2. For all-optical bistable switching, the operating wavelengths are chosen at 10% and 20% reflection as depicted in the inset of Fig. 5. Figures 5(a)–5(c) show the all-optical bistable switching behaviors of DLSWGs with the slit

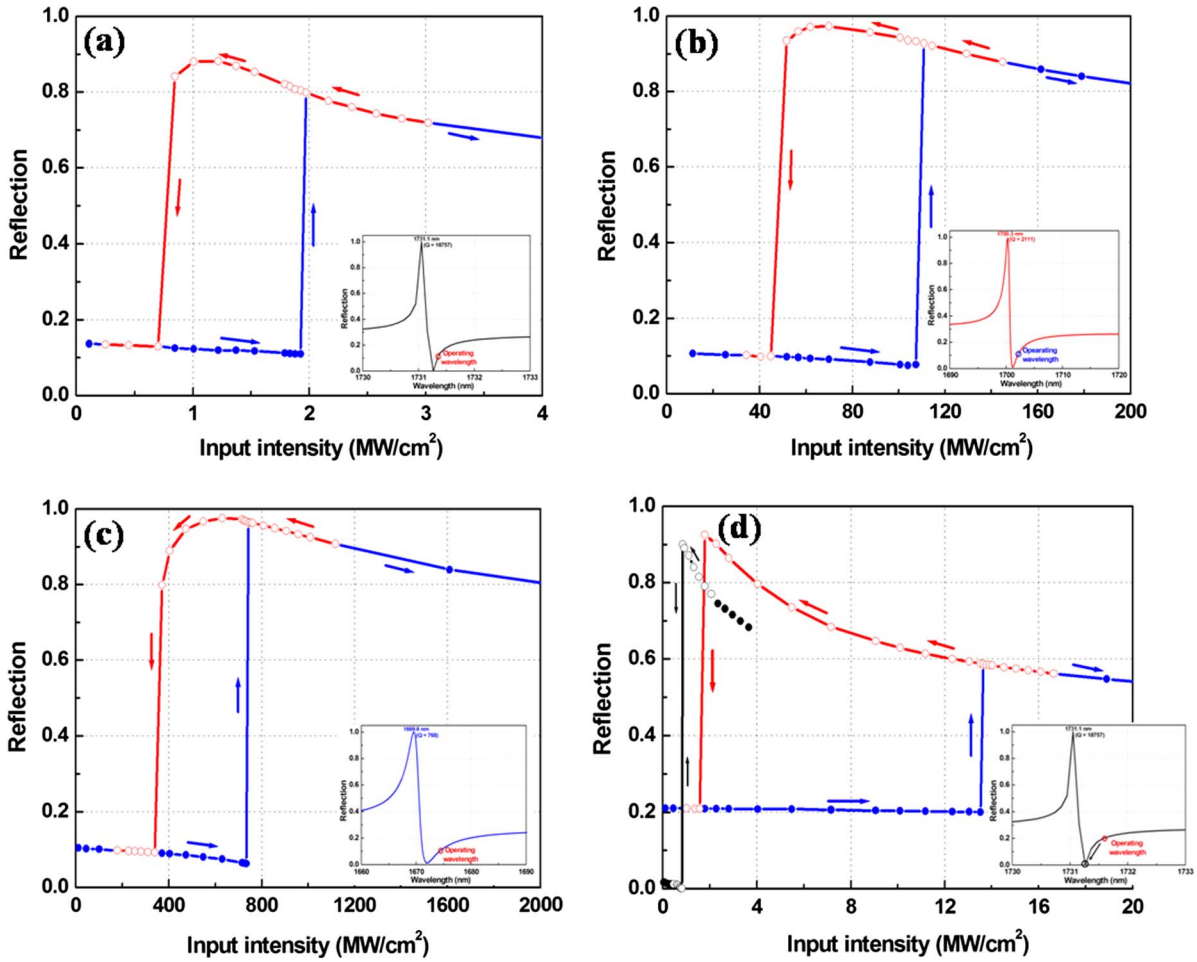


Fig. 5. All-optical bistable switching behaviors of the DLSWGs with (a) $w = 15$ nm, (b) $w = 30$ nm, and (c) $w = 45$ nm for the longer resonant region with the operating wavelength at 10% reflection and (d) at 20% [blue (right) and red (left) curves in (a), (b), and (c), and right and middle, respectively in (d)] and at the depth \[black far left curves in (d)] reflection for $w = 15$ nm.

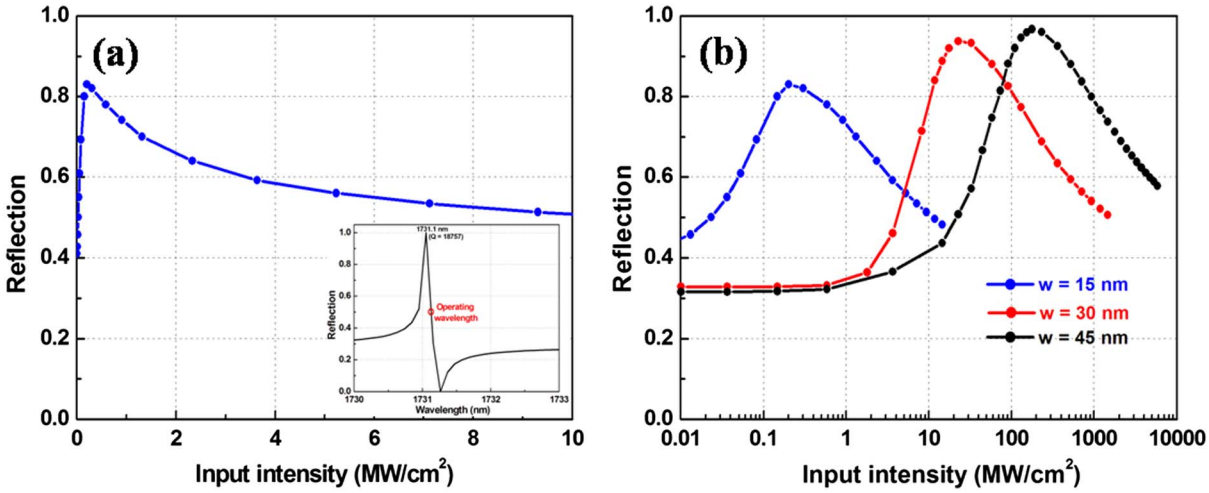


Fig. 6. (a) Switching behavior of DLSWG with the operating wavelength at 50% reflection for the slit width $w = 15$ nm and (b) All-optical switching of DLSWGs for various slit widths $w$.

widths, $w$, of 15 nm, 30 nm, and 45 nm, respectively, for the operating wavelength at 10% reflection. The bistability behavior with one switching point can be obtained in all cases. The switching intensities are 1.92 MW/cm$^2$, 104.0 MW/cm$^2$, and 733.5 MW/cm$^2$. Figure 5(d), with blue (arrows pointing up/right) and red curves (arrows pointing left/down), shows the bistability behavior with switching intensity at 13.7 MW/cm$^2$ for the operating wavelength at 20% reflection for the slit width, $w$, of 15 nm. The bandwidth of the optical bistability region is from 13.7 MW/cm$^2$ to 1.76 MW/cm$^2$. Compared to the result shown in Fig. 5(a), with the same slit width, $w$, of 15 nm and the operating wavelength apart from the resonance, the switching intensity is higher and the bandwidth of the bistability region is broader. As seen in Fig. 5, there is much more improvement of the bistability contrast for the operating wavelengths around F2 than that around F1 of the DLSWG, shown in Figs. 4(a) and 4(b) and the SLSWG shown in Figs. 2(a)–2(d). For example, for the slit width, $w = 45$ nm, of the DLSWG structure, the contrasts (low-high states) are (0.06–0.97) and (0.12–0.56) for the operating wavelengths at 10% reflection around F2 and 50% reflection around F1, respectively. For the results shown in the SLSWG for the slit width, $w = 45$ nm, with the operating wavelength at ~50% reflection, the contrast is (0.14–0.58). In addition, with the operating wavelength at the depth of resonance, the bistability behavior has not occurred, as seen in Fig. 5(d) (black vertical curves, on left) even the switching point at 0.9 MW/cm$^2$ of input intensity and high contrast is observed.

Next, we consider the operating wavelength between the peak (total reflection) and depth (zero reflection) of F2 noted in the inset of Fig. 6(a). Figure 6(a) shows the nonlinear behaviors for the DLSWG having the slit width, $w$, of 15 nm at the operating wavelength at 50% reflection. It is seen that bistability behavior does not occur at this operating wavelength. Other operating wavelengths between the peak and depth of F2 that do not offer the bistability behaviors are also treated. However, there is a critical point of the input intensity at which the reflection switches from "raising mode" to "falling mode" when increasing the input intensity. The switching intensity for the grating with the slit width, $w$, of 15 nm operating at this wavelength is 0.2 MW/cm$^2$, which is much smaller than that operating at the wavelength used in the previous calculations shown in Fig. 5(a). Figure 6(b) shows the nonlinear behavior for various slit widths. It is seen that the switching intensities for the slit widths, $w$, of 30 nm and 45 nm are 23.0 MW/cm$^2$, and 185.6 MW/cm$^2$, respectively. Compared to the results shown in Fig. 5, these switching intensities are much smaller. Thus, if we design the optical switching devices based on the Fano resonance, as in [26], the operating wavelength between the peak and the depth is preferred. Since nonlinear behaviors at the operating wavelengths in the right and left sides of the depth are different, the bistability behavior depends strongly on the operating wavelength in each resonance.

Experimentally, it is possible to fabricate our designed DLSWG using electron-beam (e-beam) lithography and inductively coupled plasma etching (ICP) techniques. In particular, two $As_2S_3$ thin films with thicknesses of 220 nm and a $SiO_2$ buffer layer are deposited on a glass substrate using RF/DC sputtering techniques. To fabricate grating structures, the three-layer film is coated by an e-beam resist layer with a thickness of ~300 nm. The gratings with the slit width and periodicity of $w$ (15 nm, 30 nm, and 45 nm) and 860 nm, respectively, are patterned on the e-beam resist layer by an e-beam lithography system. The samples are then etched by an ICP dry etcher using a mixture of $CHF_3$ and $O_2$ gases. The device structures are finally formed after removing the e-beam resist layer.

## 4. CONCLUSION

In conclusion, we have investigated the all-optical bistable switching based on Fano resonances in the single- and double-layer nonlinear slab waveguide gratings with narrow slits. The optimal SLSWG in this work shows that the switching intensity and the quality factor are better than previous results presented by other authors. Furthermore, we have demonstrated that the proposed DLSWG provided high all-optical bistable switching efficiency in terms of low switching intensity and high contrast of low and high states at the second Fano resonance in the reflection spectrum corresponding to the longer resonant wavelength. We believe that our simulation results suggest a better way to design all-optical bistable switching devices based on Fano resonances than those based on guided-mode resonances.

## ACKNOWLEDGMENTS

The authors gratefully appreciate Prof. Acad. Nguyen Van Hieu, Vietnam Academy of Science and Technology (VAST) for his generous support. This research is funded by the project of VAST under grant VAST03.06/13-14.

## REFERENCES

1. H. M. Gibbs, *Optical Bistability: Controlling Light with Light* (Academic, 1985).
2. M. Soljacic, M. Ibanescu, S. G. Johnson, Y. Fink, and J. D. Joannopoulos, "Optimal bistable switching in nonlinear photonic crystals," Phys. Rev. E **66**, 055601(R) (2002).
3. S. F. Mingaleev, A. E. Miroshnichenko, and Yu. S. Kivshar, "Coupled-resonator-induced reflection in photonic-crystal waveguide structures," Opt. Express **16**, 11647–11659 (2008).
4. K. Nozaki, A. Shinya, S. Matsuo, T. Sato, E. Kuramochi, and M. Notomi, "Ultralow-energy and high-contrast all-optical switch involving Fano resonance based on coupled photonic crystal nanocavities," Opt. Express **21**, 11877–11888 (2013).
5. L. Y. Mario, S. Darmawan, and M. K. Chin, "Asymmetric Fano resonance and bistability for high extinction ratio, large modulation depth, and low power switching," Opt. Express **14**, 12770–12781 (2006).
6. Q. M. Ngo, S. Kim, S. H. Song, and R. Magnusson, "Optical bistable devices based on guided-mode resonance in slab waveguide gratings," Opt. Express **17**, 23459–23467 (2009).
7. Q. M. Ngo, K. Q. Le, and V. D. Lam, "Optical bistability based on guided-mode resonances in photonic crystal slabs," J. Opt. Soc. Am. B **29**, 1291–1295 (2012).
8. Q. M. Ngo, T. T. Hoang, V. L. Nguyen, D. L. Vu, and V. H. Pham, "Metallic assisted guided-mode resonances in slab waveguide gratings for reduced optical switching intensity in bistable devices," J. Opt. **15**, 055503 (2013).
9. J. A. Porto, L. Martin-Moreno, and F. J. Garcia-Vidal, "Optical bistability in subwavelength slit apertures containing nonlinear media," Phys. Rev. B **70**, 081402(R) (2004).
10. A. E. Miroshnichenko, S. Flach, and Yu. S. Kivshar, "Fano resonances in nanoscale structures," Rev. Mod. Phys. **82**, 2257–2298 (2010).
11. C. Grillet, D. Freeman, B. Luther-Davies, S. Madden, R. McPhedran, D. J. Moss, M. J. Steel, and B. J. Eggleton, "Characterization and modeling of Fano resonances in chalcogenide photonic crystal membranes," Opt. Express **14**, 369–376 (2006).
12. M. Heuck, P. T. Kristensen, Y. Elesin, and J. Mørk, "Improved switching using Fano resonances in photonic crystal structures," Opt. Lett. **38**, 2466–2468 (2013).
13. B. Luk'yanchuk, N. I. Zheludev, S. A. Maier, N. J. Halas, P. Nordlander, H. Giessen, and C. T. Chong, "The Fano resonance in plasmonic nanostructures and metamaterials," Nat. Mater. **9**, 707–715 (2010).
14. L. Chen, Z. Qiang, H. Yang, H. Pang, Z. Ma, and W. Zhou, "Polarization and angular dependent transmissions on transferred nanomembrane Fano filters," Opt. Express **17**, 8396–8406 (2009).
15. Y. Shuai, D. Zhao, Z. Tian, J.-H. Seo, D. V. Plant, Z. Ma, S. Fan, and W. Zhou, "Double-layer Fano resonance photonic crystal filters," Opt. Express **21**, 24582–24589 (2013).
16. Y. Shuai, D. Zhao, A. S. Chadha, J.-H. Seo, H. Yang, S. Fan, Z. Ma, and W. Zhou, "Coupled double-layer Fano resonance photonic crystal filters with lattice-displacement," Appl. Phys. Lett. **103**, 241106 (2013).
17. K.-L. Lee, S.-H. Wu, C.-W. Lee, and P.-K. Wei, "Sensitive biosensors using Fano resonance in single gold nanoslit with periodic grooves," Opt. Express **19**, 24530–24539 (2011).
18. S. Boutami, B. B. Bakir, H. Hattori, X. Letartre, J.-L. Leclercq, P. Rojo-Romeo, M. Garrigues, C. Seassal, and P. Viktorovitch, "Broadband and compact 2-D photonic crystal reflectors with controllable polarization dependence," IEEE Photon. Technol. Lett. **18**, 835–837 (2006).
19. S.-L. Chua, Y. Chong, A. D. Stone, M. Soljacic, and J. Bravo-Abad, "Low-threshold lasing action in photonic crystal slabs enabled by Fano resonances," Opt. Express **19**, 1539–1562 (2011).
20. G. D'Aguanno, D. de Ceglia, N. Mattiucci, and M. J. Bloemer, "All-optical switching at the Fano resonances in subwavelength gratings with very narrow slits," Opt. Lett. **36**, 1984–1986 (2011).
21. H. Duan, D. Winston, J. K. W. Yang, B. M. Cord, V. R. Manfrinato, and K. K. Berggren, "Sub-10-nm half-pitch electron-beam lithography by using PMMA as a negative resist," J. Vac. Sci. Technol. B **28**, C6C58–C6C62 (2010).
22. H. Y. Song, S. Kim, and R. Magnusson, "Tunable guided-mode resonances in coupled gratings," Opt. Express **17**, 23544–23555 (2009).
23. A. Taflove, *Computational Electrodynamics* (Artech House, 1995).
24. A. Farjadpour, D. Roundy, A. Rodriguez, M. Ibanescu, P. Bermel, J. D. Joannopoulos, S. G. Johnson, and G. Burr, "Improving accuracy by subpixel smoothing in FDTD," Opt. Lett. **31**, 2972–2974 (2006).
25. J. M. Laniel, N. Ho, and R. Vallee, "Nonlinear-refractive-index measurement in $As_2S_3$ channel waveguides by asymmetric self-phase modulation," J. Opt. Soc. Am. B **22**, 437–445 (2005).
26. S. Carretero-Palacios, A. Minovich, D. N. Neshev, Yu. S. Kivshar, F. J. Garcia-Vidal, L. Martin-Moreno, and S. G. Rodrigo, "Optical switching in metal-slit arrays on nonlinear dielectric substrates," Opt. Lett. **35**, 4211–4213 (2010).